Original Article

MOLECULAR METABOLISM

Hepatic glycogenolysis is determined by maternal high-calorie diet *via* methylation of *Pygl* and it is modified by oteocalcin administration in mice

Tomoyo Kawakubo-Yasukochi [1,*,7], Ena Yano [1], Soi Kimura [1,3], Takuya Nishinakagawa [2], Akiko Mizokami [1], Yoshikazu Hayashi [4], Yuji Hatakeyama [4], Kenji Ohe [5], Atsushi Yasukochi [3], Seiji Nakamura [3], Eijiro Jimi [1], Masato Hirata [6,]**

ABSTRACT

Objective: Accumulating evidence indicates that an adverse perinatal environment contributes to a higher risk of metabolic disorders in the later life of the offspring. However, the underlying molecular mechanisms remain largely unknown. Thus, we investigated the contribution of maternal high-calorie diet and osteocalcin to metabolic homeostasis in the offspring.

Methods: Eight-week-old C57Bl/6N female mice were mated with age-matched males and allocated randomly to three groups: a normal-diet (ND) or a high-fat, high-sucrose diet group, which was administered either saline (control) or GluOC (10 ng/g body mass) from the day of mating to that of delivery, and the dams were fed a ND after the delivery. Pups weaned at 24 days after birth were analyzed.

Results: A maternal high-fat, high-sucrose diet during pregnancy causes metabolic disorders in the liver of the offspring *via* hypermethylation of the *Pygl* gene, encoding glycogen phosphorylase L, which mediates hepatic glycogenolysis. The reduced expression of Pygl induced by the maternal diet causes the hepatic accumulation of glycogen and triglyceride in the offspring, which remains in adulthood. In addition, the administration of uncarboxylated osteocalcin during pregnancy upregulates *Pygl* expression *via* both direct CREBH and ATF4 and indirect epigenomic pathways, mitigating the maternal diet-induced obesity and abnormal glucose and lipid metabolism in adulthood.

Conclusions: We propose that maternal energy status is reflected in the hepatic glycogenolysis capacity of the offspring *via* epigenetic modification of *Pygl* and uncarboxylated osteocalcin regulates glycogenolysis.

Keywords *Pygl*; *Ahr*; Glycogen; DNA methylation; Osteocalcin; Developmental origins of health and disease

1. INTRODUCTION

Non-communicable diseases (NCDs), particularly those classified as NCD4, which includes cancer, diabetes, cardiovascular disease, and chronic respiratory disease, have emerged as the leading cause of human morbidity and mortality worldwide [1]. Unhealthy diets, physical inactivity, excess alcohol consumption, and exposure to tobacco smoke have been identified as the four most common and preventable risk factors that contribute to the etiology of NCDs. Of these, nutritional status is considered the most difficult to tackle. In addition to such diets having effects on the individual consuming them, it is well known that nutrition during pregnancy and early life plays an important role in fetal and neonatal growth and development [2]. Moreover, recent studies have shown that improper nutritional status during pregnancy can cause chronic metabolism-related disorders in the offspring, predisposing individuals toward NCDs in later life [1]. This concept is currently referred to as the Developmental Origins of Health and Disease (DOHaD) [2].

The effects of maternal nutrition on the offspring are thought to be mediated *via* epigenetic mechanisms, such as DNA methylation,

[1]OBT Research Center, Faculty of Dental Science, Kyushu University, 3-1-1 Maidashi, Higashi-ku, Fukuoka 812-8582, Japan [2]Department of Immunological and Molecular Pharmacology, Faculty of Pharmaceutical Sciences, Fukuoka University, 8-19-1 Nanakuma, Jonan-ku, Fukuoka 814-0180, Japan [3]Section of Oral and Maxillofacial Oncology, Division of Maxillofacial Diagnostic and Surgical Sciences, Faculty of Dental Science, Kyushu University, 3-1-1 Maidashi, Higashi-ku, Fukuoka 812-8582, Japan [4]Division of Functional Structure, Department of Morphological Biology, Fukuoka Dental College, 2-15-1 Tamura, Sawara-ku, Fukuoka 814-0193, Japan [5]Department of Pharmacotherapeutics, Faculty of Pharmaceutical Sciences, Fukuoka University, 8-19-1 Nanakuma, Jonan-ku, Fukuoka 814-0180, Japan [6]Oral Medicine Research Center, Fukuoka Dental College, 2-15-1 Tamura, Sawara-ku, Fukuoka 814-0193, Japan

[7] Former affiliation of the author: Department of Immunological and Molecular Pharmacology, Faculty of Pharmaceutical Sciences, Fukuoka University, 8-19-1 Nanakuma, Jonan-ku, Fukuoka 814-0180, Japan.

*Corresponding author. E-mail: tomoyo@dent.kyushu-u.ac.jp (T. Kawakubo-Yasukochi).

**Corresponding author. E-mail: hirata@college.fdcnet.ac.jp (M. Hirata).

Received September 19, 2021 • Revision received October 11, 2021 • Accepted October 17, 2021 • Available online 19 October 2021

https://doi.org/10.1016/j.molmet.2021.101360

histone modification, non-coding RNAs, and nucleosome remodeling [2]. Most epigenetic studies regarding the developmental programming of metabolic disorders have focused on DNA methylation [3,4]. However, little is known regarding how the DNA methylation status of specific genes, established during early life, could affect the developmental programming of NCDs.

Osteocalcin (OC), the most abundant non-collagenous protein in bone, is produced by osteoblasts [5]. It undergoes vitamin K-dependent post-translational γ-carboxylation to produce Carboxylated OC or Gla-protein (GlaOC), which is deposited in the bone matrix, but a small proportion of the OC remains uncarboxylated (GluOC). Furthermore, GlaOC can be decarboxylated to yield GluOC in the process of osteolysis, which is performed by activated osteoclasts. Many recent studies have shown that GluOC can ameliorate diabetes by affecting multiple aspects of systemic glucose and energy metabolism [6—12] through a mechanism that is dependent on the interaction with its putative receptor G protein-coupled **receptor**, class C, group 6, member A (GPRC6A) [13].

In our previous study, we demonstrated that the feeding of a high-fat, high-sucrose (HFS) diet to mice during pregnancy increases body mass gain and induces metabolic disorders in the offspring after weaning, especially in female mice, while the oral administration of GluOC to the mothers during gestation reduces obesity and metabolic disorders in their offsprings [14]. We hypothesize that an *in utero*-inherited epigenetic mechanism might influence the phenotypes of the offspring. Therefore, in the present study, we aimed to identify the mechanisms underpinning the phenotype of the offspring by comparing the hepatic DNA methylation status of the offspring of mice fed a normal diet (ND) or an HFS, referred to as ND-offspring and HFS-offspring, respectively. In addition, we aimed to determine how GluOC administration rescues the metabolism of HFS-offspring. We conclude that *Pygl* expression is epigenetically suppressed through DNA hypermethylation of the transcriptional promoter region of the gene *in utero*. We also show that maternal GluOC administration prevents this aberrant glycogen metabolism in the offspring by reducing the methylation of the promoter region of *Pygl* and inducing endogenous hepatic GluOC synthesis, which upregulates Pygl expression and activity.

2. MATERIALS AND METHODS

2.1. Animal experiments

The study protocol was approved by the Animal Care and Use Committee of Fukuoka University (permission nos. 1703029, 1815121, and 1906021). The experimental protocol is shown in Figure 1A.

2.2. Cells

Mouse hepatoma Hepa1c1c7 cells [15], obtained from the ECACC (Salisbury, UK), were maintained in alpha minimum essential medium without nucleosides (Fujifilm Wako, Osaka, Japan) that contained 10% fetal bovine serum (Biowest, Nuaillè, France) and 1% penicillin and streptomycin (Nacalai Tesque, Kyoto, Japan) under a humidified atmosphere of 5% CO_2 at 37 °C.

2.3. Illumina hiseq sequencing and data analysis

Whole-genome bisulfite sequencing and data analysis were performed by Cell Innovator Inc. (Fukuoka, Japan). Mouse genomic DNA was purified using NucleoSpin Tissue (Takara Bio, Shiga, Japan) and treated with bisulfite using an EZ DNA Methylation-Gold Kit (Zymo Research, Irvine, CA). Bisulfite sequencing libraries were then prepared using a TruSeq DNA Methylation Kit (Illumina, San Diego, CA), according to the manufacturer's instructions. Cluster amplification and 151 bp paired-end sequencing were performed, following the manufacturer's protocol (Illumina) for HiSeqX (Illumina). After sequencing, the raw sequence reads were filtered on the basis of quality using FastQC (http://bioinformatics.babraham.ac.uk/projects/fastqc/). The adapter sequences were also trimmed off the raw sequence reads using trimmomatic v0.32 [16]. The trimmed reads were mapped to the reference genome using whole genome Bisulfite Sequence Mapping Program (BSMAP) [17] which is based on the Short Oligo Alignment Program [18]. The methylation ratio of every single cytosine location was extracted from the mapping results using the 'methylatio.py' script in BSMAP.

To identify the significantly over-represented GO categories and significantly enriched pathways, we used tools and data provided by the *Database for Annotation, Visualization and Integrated Discovery* (DAVID) (https://david.ncifcrf.gov).

2.4. Validation of bisulfite sequencing

Mouse genomic DNA, purified using NucleoSpin Tissue (Takara Bio, Japan), was treated with bisulfite using a MethylEasy Xceed Rapid DNA Bisulphite Modification Kit (Takara Bio) and purified, according to the manufacturer's instructions. The bisulfite-treated sequences of the promoter region of each gene were amplified by TaKaRa EpiTaq HS (Takara Bio) using sense- and antisense-specific primer sets (Supplementary Table 1), under the following PCR conditions: 40 cycles of 10 s at 98 °C, 30 s at 52 °C (for *Pygl*) or 56 °C (for *Ocn*), and 30 s at 72 °C. The amplified fragments were ligated into pT7Blue T-vector (Merck Millipore, Burlington, MA), and more than eight clones were sequenced per reaction (Unitech, Chiba, Japan).

2.5. Histological analysis

Tissue samples were embedded in paraffin and stained using hematoxylin and eosin (HE) used for immunohistochemistry (performed by Morphotechnology Co. Ltd., Sapporo, Japan) using primary antibodies against Pygl (diluted 1:75, Cat# Ab198268, Abcam, Cambridge, UK) or osteocalcin (diluted 1:1,000, Cat# Ab198268, Abcam), for 1 h at room temperature, according to the polymer method. Periodic acid-Schiff (PAS) staining, along with amylase digestion, was performed as previously described [19].

2.6. Determination of hepatic glycogen and free glucose contents

The glycogen content of the liver was measured using a Glycogen Colorimetric Assay Kit II (BioVision, Milpitas, CA), according to the manufacturer's instructions [20]. Briefly, freshly isolated mouse liver samples were homogenized in distilled water and incubated for 10 min on ice, then boiled for 10 min at 95 °C. The samples were then centrifuged at 20,000 × *g* for 10 min and the supernatants were collected and analyzed. Hydrolysis enzyme mix (2 μl) was added to an aliquot of each standard/sample (50 μl/well) in a 96-well plate and the mixtures were incubated for 30 min at room temperature. After adding the reaction mix to each well, the samples were incubated for a further 30 min at room temperature. Finally, the amount of glycogen in each sample was determined at 450 nm using an iMark plate reader (Bio-Rad, Hercules, CA) and dilutions of a standard glycogen preparation. Free glucose content was measured using a D-glucose assay kit (Megazyme, Chicago, IL), according to the manufacturer's instructions [20]. The glycogen and free glucose contents were normalized to the protein concentrations of the samples, measured using a BCA Protein assay kit (Fujifilm Wako).

2.7. Measurement of blood glucose concentration

Blood samples were obtained by tail-tip amputation and their glucose concentrations were measured using a FreeStyle Freedom meter (Abbott Laboratories, Abbott Park, IL).

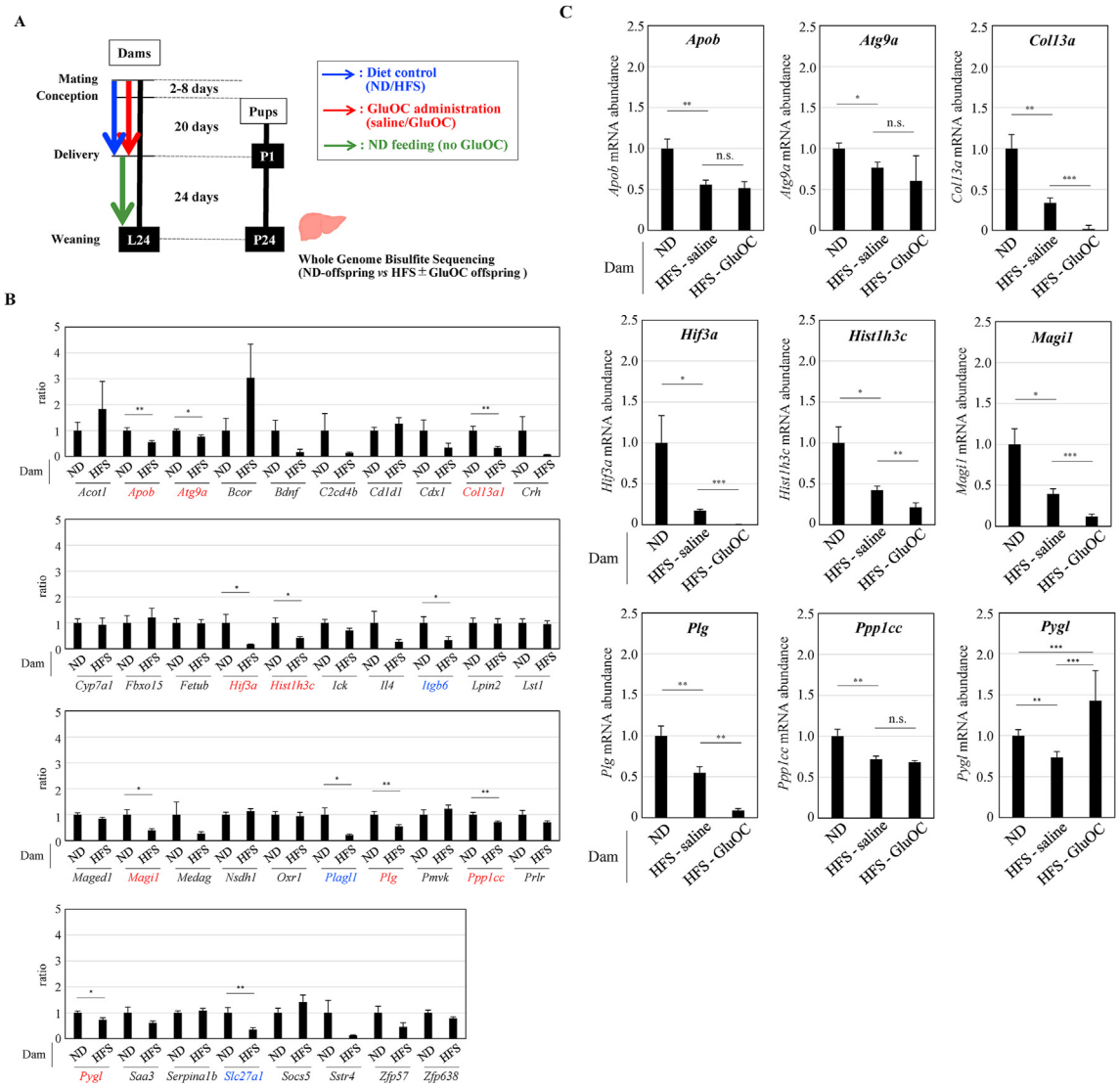

Figure 1: Experimental protocol and whole-genome bisulfite sequence (WGBS) analysis. (A) Experimental protocol. Female 8-week-old C57Bl/6N mice were mated with age-matched males and allocated randomly to three groups: a normal diet (ND) group or a high-fat, high-sucrose diet (HFS, F2HFHSD, Oriental Yeast, Tokyo, Japan; containing 20% sucrose and 30% fat) group, which was administered either saline (control) or GluOC (10 ng/g body mass) from the day of mating to that of delivery, and the dams were fed ND after the delivery. The offspring groups were designated as ND-, HFS-saline-, and HFS-GluOC-offspring, according to the diet and GluOC administration status of their dams determined during pregnancy. Tissues and blood were collected without fasting. (B) Quantitative RT-PCR analysis of 38 metabolic genes that had significantly differently methylated promoters in HFS-offspring, according to WGBS analysis. Of these, nine genes (red-colored) displayed lower mRNA expression and hypermethylation of their promoters: *Apob* (apolipoprotein B), *Atg9a* (autophagy-related 9A), *Col13a1* (collagen type 13 alpha 1 chain), *Hif3a* (hypoxia-inducible factor 3 alpha subunit), *Hist1h3c* (histone cluster 1H3 family member C), *Magi1* (membrane-associated guanylate kinase, WW and PDZ domain-containing 1), *Plg* (plasminogen), *Ppp1cc* (protein phosphatase 1 catalytic subunit gamma), and *Pygl* (glycogen phosphorylase L). In addition, there were three genes for which the promoter methylation in the HFS-fed samples was lower (blue-colored): *Itgb6* (integrin beta 6), *Plagl1* (pleomorphic adenoma gene-like 1), and Slc27a1 (solute carrier family 27, member 1). (C) Quantitative RT-PCR analysis of the above nine genes in the livers of the offspring from the three groups. RNA (n = 12 per group) was extracted from the P24 mouse liver and the expression of *Actb* was determined as the reference gene. Data are expressed as mean ± SEM of three independent experiments. Student's *t*-test (A) or one-way ANOVA and Dunnett's *post-hoc* test (C) were used. $*P < 0.05$, $**P < 0.01$, $***P < 0.001$; n.s., not significant.

2.8. ELISA for OC

Levels of GlaOC or GluOC were measured using Mouse Gla- or Glu-OC High-sensitivity EIA kits (Takara Bio, MK127 or 129), respectively).

2.9. Measurement of serum and hepatic triglyceride concentrations

Serum and hepatic triglyceride concentrations were measured using a Fuji Dri-Chem analyzer (Fujifilm, Tokyo, Japan) and Fuji Dri-Chem slides (TG-P III, Fujifilm). Serum samples were directly applied to the slides. For hepatic triglyceride measurements, fresh liver samples were weighed, rapidly homogenized in 700 μl of chloroform/methanol mixture (2:1, v/v), and incubated for 2 h at room temperature. After centrifugation at 15,000 rpm for 5 min at 4 °C, the supernatants were transferred to new 1.5-ml tubes. Following air-drying overnight, the lipids were dissolved in 90 μl isopropanol, then centrifuged at 15,000 rpm for 5 min at 4 °C. The supernatants were collected, their volumes measured, and they were stored at −20 °C until analyzed further. The samples were diluted 20 times in PBS immediately before application to a slide.

2.10. Measurement of the Pygl activity

The enzymatic activity of Pygl was measured using a Glycogen Phosphorylase Colorimetric Assay Kit (BioVision, Milpitas, CA), according to the manufacturer's protocol. Briefly, fresh liver samples were rapidly homogenized in 200 μl ice-cold Assay buffer and incubated for 15 min on ice. After centrifugation at 15,000 rpm for 15 min at 4 °C, the supernatants were collected and stored at −20 °C until analyzed. Each standard or sample (50 μl) was placed in a 96-well plate, and then 50 μl Reaction mix containing Assay buffer, glycogen, Enzyme mix, Developer, and Substrate Mix was added, followed by incubation for 1 h at 30 °C. Finally, absorbance was measured at 450 nm using an iMark plate reader (Bio-Rad). Standard curves for determining the quantities of G1P were prepared by diluting the G1P standard. Pygl activity was normalized to the protein concentrations of the samples, measured using a BCA Protein assay kit (Fujifilm Wako).

2.11. Quantitative PCR analysis

RNA was extracted from tissues using Sepasol-RNA I Super G (Nacalai Tesque) and a High Pure RNA Isolation Kit (Roche Diagnostics, Mannheim, Germany). The RNA was reverse transcribed using a Verso cDNA Synthesis Kit (Thermo Fisher Scientific), and the resulting complementary DNA (cDNA) was subjected to two-step qPCR analysis using a LightCycler 480 system (Roche Diagnostics). For the TaqMan method, the cycling conditions were as follows: 95 °C for 10 min (hot-start quantitative polymerase chain reaction-qPCR), followed by 45 cycles of 95 °C for 15 s, 60 °C for 30 s, and 72 °C for 1 s. The PCR primer sequence probes specific for each sequence (Roche Diagnostics), and amplicon sizes are listed in Supplementary Table 2. For the SYBR Green method, the cycling conditions were as follows: 95 °C for 10 min (hot-start PCR), followed by 40 cycles of 95 °C for 5 s and 58 °C for 30 s. The PCR primer sequences and amplicon sizes are listed in Supplementary Table 3.

2.12. Immunoblot analysis

Cells or tissues were lysed and homogenized in Radioimmunoprecipitation (RIPA) buffer (Fujifilm Wako Pure Chemical) containing a protease inhibitor cocktail (Nakalai Tesque). After centrifugation, the supernatants were collected and the protein concentrations of the samples determined using a BCA Protein assay kit (Fujifilm Wako Pure Chemical). Each sample (25 μg/tube) was supplemented with SDS-PAGE sample buffer containing 2-mercaptoethanol (Nakalai Tesque), incubated at 95 °C for 5 min, and then separated by glycine-based 5–20% or tricine-based 15–20% gradient SuperSep precast gels (Fujifilm Wako). The separated proteins were transferred onto Immobilon PVDF membranes (Merck Millipore) and non-specific protein binding was blocked using Blocking One (Nakalai Tesque) for 1 h at room temperature. The following primary antibodies were used: anti-Pygl (diluted 1:3,000, Cat# Ab198268, Abcam), anti-osteocalcin (diluted 1:2,000, Cat# Ab198268, Abcam), anti-Ahr (diluted 1:5,000, Cat# BML-SA550, Enzo Biochem, Farmingdale, NY), anti-Gprc6a (diluted 1:1,000, Cat# sc-67302, Santa Cruz Biotechnology, Dallas, TX), anti-Creb3l3 (diluted 1:2,000, Cat# sc-377331, Santa Cruz Biotechnology), anti-Atf4 (diluted 1:2,000, Cat# 10835, Proteintech, Rosemont, IL), and anti-β-actin (diluted 1:40,000, Cat# M177-3, MBL, Nagoya, Japan). After incubation with the primary antibody at 4 °C overnight, the membranes were washed with Tris-buffered saline containing 0.1% Tween-20 (Fujifilm Wako Chemicals Corporation) and incubated with the appropriate secondary antibodies coupled to HRP: anti-rabbit (diluted 1:5,000, Cell Signaling Technology, Danvers, MA) for Pygl, osteocalcin, and Ahr; and anti-mouse (diluted 1:40,000, Cell Signaling Technology) for β-actin for 6 h at 4 °C. After washing, the membranes were analyzed using the ImageQuant LAS4000 system (GE Healthcare, Chicago, IL) after incubation with Amersham ECL reagent (Cytiva, Tokyo, Japan).

2.13. Small interfering RNA (siRNA) transfection

Duplexed siRNA sets for *Ahr*, *Gprc6a*, *Creb3l3*, and *Atf4* were purchased from Bioneer (Daejeon, South Korea) and/or Sigma–Aldrich (St. Louis, MO): 11622-2-B and SASI_Mm01_00168275 for *Ahr*, SASI_Mm01_00129328 and SASI_Mm01_00129329 for *Gprc6a*, SASI_Mm02_00340645 and SASI_Mm01_00124399 for *Creb3l3*, and SASI_Mm02_00316863 and SASI_Mm02_00316864 for *Atf4*. Control siRNA was purchased from Sigma–Aldrich (Cat# SIC-001). mRNA or protein expression was measured in Hepa1c1c7 cell lysates 24–48 h after siRNA transfection with Lipofectamine RNAiMAX (Thermo Fisher Scientific).

2.14. Luciferase assay

To construct the *Pygl* gene promoter-driven reporter plasmid (pGL4.10-Pygl-wt), the 5′-flanking region from −932 nt to −20 nt of the mouse *Pygl* gene was amplified from mouse cDNA by PCR. The PCR products were digested using KpnI and BglII and cloned into the same sites of the pGL4.10 vector (Promega, Madison, WI). Site-specific mutations were introduced into the promoter construct using an In-Fusion HD Cloning Kit (Takara Bio), Max Efficiency DH10B Competent cells (Thermo Fisher Scientific), the Wizard SV Gel, and PCR Clean-Up System (Promega), and Tks Gflex DNA Polymerase (Takara Bio, Japan). The identity of the cloned plasmid was verified by sequence analysis (Kazusa Genome Technologies, Chiba, Japan). The luciferase assays were performed using the Dual-Glo Luciferase Assay System (Promega). Briefly, 1.5×10^4 cells were seeded in clear-bottomed, white 96-well plates (Greiner Bio-One, Frickenhausen, Germany) and incubated under a humidified atmosphere of 5% CO_2 at 37 °C overnight. One hundred twenty-five nanograms pGL4.10 plasmid (Pygl-wild, XRE1mut, XRE2mut, or XRE1/2dmut) and 65 ng pRL plasmid (Promega) were transiently co-transfected into Hepa1c1c7 cells using Lipofectamine 3000 reagent (Thermo Fisher Scientific). After 24 h, the volume of the medium was adjusted to 75 μl in each well and Dual-Glo reagent (75 μl) was added. The cells were gently agitated for ≥20 min to ensure lysis. The luminescence of each well was measured in a luminescence-equipped plate reader (ALVO X3, PerkinElmer, Waltham, MA). Next, 75 μl per well Stop-Glo reagent was added to each well to quench the luciferase reaction and begin the *Renilla* luminescence, then the luminescence of each well was measured again. The data are shown as the first luminescence value (luciferase) divided by the second value (*Renilla*).

2.15. ChIP-qPCR assay

ChIP assays were performed using formalin-fixed, paraffin-embedded (FFPE) samples, a ChIP-IT FFPE Chromatin Preparation Kit (Active Motif, Carlsbad, CA), and a ChIP-IT FFPE II Kit (Active Motif). Briefly, for chromatin preparation, six 15-μm sections from each FFPE tissue block were used as the starting materials. After paraffin removal, the tissue was rehydrated and then incubated in Lysis Buffer containing a protease inhibitor cocktail and RNaseA, followed by digestion with Enzymatic Shearing Cocktail. After centrifugation, all the remaining sample was pooled into a single tube for sonication (Bioruptor; Diagenode, Seraing, Belgium). After the final centrifugation, the soluble and insoluble chromatin was analyzed and quantified by qPCR using an *Actb* primer set (Supplementary Table 4), to confirm whether most of the chromatin had been extracted. qPCR analysis was performed using

LightCycler480 SYBR Green I Master (Roche Diagnostics) and the following cycling conditions: 95 °C for 5 min, followed by 40 cycles of 95 °C for 10 s, 58 °C for 30 s, and 72 °C for 30 s. For the next step using a ChIP-IT FFPE II Kit, chromatin (200 ng/reaction) was pre-cleaned, then incubated with an antibody against the appropriate DNA-binding protein. The antibody-bound protein/DNA complexes were immunoprecipitated using Protein G agarose beads and washed by gravity filtration. Following immunoprecipitation, cross-linking was inhibited, the proteins were removed by Protease K digestion, and the DNA was purified. ChIP-enriched DNA samples were used for qPCR alongside primer sets for *Pygl* (Supplementary Table S4). The antibodies used in the ChIP assay were anti-TET1 (diluted 1:100, GeneTex, Irvine CA), anti-TET2 (diluted 1:100, Proteintech), anti-TET3 (diluted 1:100, GeneTex), anti-DNMT3A (diluted 1:100, Cell Signaling Technology), and anti-DNMT3B (diluted 1:100, Cell Signaling Technology).

2.16. Intracellular cAMP quantification

The intracellular cAMP concentration was measured using a Direct cAMP ELISA kit (Enzo Life Sciences), according to the manufacturer's instructions. Hepa1c1c7 cells were seeded in 6-well plates (1.5×10^5 cells/well) and incubated under a humidified atmosphere of 5% CO_2 at 37 °C for 48 h. After treatment with 0–50 ng/ml GluOC or 50 μM forskolin (Merck Millipore) for 15 min, the cells were lysed using 0.1 M HCl to stop endogenous phosphodiesterase activity and to stabilize the released cAMP protein. The HCl-treated samples were then collected, acetylated to increase sensitivity, and neutralized using the dedicated reagents in the kit. They were then placed into the supplied pre-coated ELISA plate, reacted, and absorbance was measured at 405 nm.

2.17. Statistical analysis

Student's *t*-test or ANOVA followed by Dunnett's test were performed as appropriate, using JMP software (ver14; Cary, NC, USA). All quantitative data are summarized as mean ± standard error of the mean. $P < 0.05$ was considered to represent statistical significance.

3. RESULTS

3.1. Comprehensive whole-genome bisulfite sequencing (WGBS) of the livers of ND- and HFS-offspring on postnatal day 24

Experiments were performed according to the protocol shown in Figure 1A, using female mice because the beneficial effects of GluOC administration during pregnancy on the metabolism of mature offspring were most pronounced in the female mice [14]. Because of the similarity of the metabolic profiles of the mature female offspring of dams fed a normal diet (ND), and to determine whether their mothers were administered GluOC or not [14], we studied ND-saline-offspring (as ND-offspring) alone in the present study. To determine the effect of feeding an HFS diet to pregnant mice on the DNA methylation status of the offspring, WGBS was performed on the livers of female ND- and HFS-offspring collected at weaning, on a postnatal day (P) 24, when the nutritional status of the offspring would be dependent on their dams. The WGBS revealed that methylation coverage in the CG, CHC, and CHH sequence contexts were 69.81% and 68.42%, 0.76% and 0.73%, and 0.52% and 0.52% for ND- and HFS-offspring, respectively; this showed consistency with the results of a previous study which showed that methylation predominantly occurs on CpG dinucleotides in mammals [21]. The data sets generated by this analysis were submitted to the **Gene** Expression Omnibus (GEO) database (http://www.ncbi.nlm.nih.gov/geo/; accession no. GSE181760). After the data were analyzed to determine the methylation status of 35,595,501 CpG dinucleotides and the overall distribution, the nucleotides with methylation levels in the HFS-offspring that were >2-fold or <0.5-fold those of the ND-offspring were identified. Of these, we focused on the CpG methylation status of gene promoter regions (5,479 CpG dinucleotides in 933 promoters), because the DNA methylation status of gene promoters is widely recognized to influence transcription [21]. Furthermore, we performed Gene Ontology (GO) (Supplementary Table 5) and Kyoto encyclopedia of genes and genomes (KEGG) enrichment analysis (Supplementary Table 6) using the online Database for Annotation, Visualization and Integrated Discovery (DAVID) [22]. We next focused on 38 candidate genes (Figure 1B) that had GO terms related to glucose or lipid metabolic processes, and measured the expression of these 38 mRNAs by quantitative (q)RT-PCR, and found that the expression of nine target genes was significantly lower in the livers of HFS-offspring than in those of ND-offspring and that these expression levels were positively associated with promoter methylation status (hypermethylation in the HFS-offspring). These genes were *apolipoprotein B* (*Apob*), *autophagy-related 9A* (*Atg9a*), *collagen type 13 alpha 1 chain* (*Col13a1*), *hypoxia-inducible factor 3 alpha subunit* (*Hif3a*), *histone cluster 1 H3 family member C* (*Hist1h3c*), *membrane-associated guanylate kinase, WW and PDZ domain-containing 1* (*Magi1*), *plasminogen* (*Plg*), *protein phosphatase 1 catalytic subunit gamma* (*Ppp1cc*), and *glycogen phosphorylase L* (*Pygl*). In addition, the expression of three genes was inversely associated with promoter methylation status and was determined according to the WGBS analysis. These genes were *integrin beta 6* (*Itgb6*), *pleomorphic adenoma gene-like 1* (*Plagl1*), and *solute carrier family 27, member 1* (*Slc27a1*) (Figure 1B).

Our previous study demonstrated that the metabolic disorders in the mature offspring of HFS-fed dams were largely prevented by the administration of GluOC during pregnancy, such that the metabolism of these offspring was comparable to that of ND-offspring consuming the same diet [14]. Therefore, we hypothesized that one or more of the nine genes for which the DNA methylation is affected by maternal nutrition while *in utero* might influence metabolism and that their expression might be restored in GluOC-treated HFS-offspring. Therefore, another qRT-PCR analysis was performed to compare the three groups of mice: the ND-offspring, HFS-saline-offspring, and HFS-GluOC-offspring. Of the nine genes, only low *Pygl* expression in the HFS-offspring was restored (by GluOC administration during pregnancy) to a level higher than that of the ND-offspring (Figure 1C).

3.2. Pygl expression in mouse liver is regulated by the methylation status of xenobiotic response elements (XREs) in its promoter region

To validate the results of the WGBS, the hepatic *Pygl* promoter methylation status of the three groups was evaluated using bisulfite genomic sequencing (Figure 2A), focusing on the three XREs located in the *Pygl* promoter region (Supplementary Figure S1), where the methylated cytosines were concentrated in the HFS-saline-offspring, according to the results of the WGBS analysis. The proportions of the elements that were composed entirely of unmethylated cytosines were 63% and 25% (ND-offspring), 13% and 13% (HFS-saline-offspring), and 63% and 63% (HFS-GluOC-offspring) in the two CpGs in XRE-1; and 25% (ND-offspring), 13% (HFS-saline-offspring), and 63% (HFS-GluOC-offspring) for the CpG in XRE-2, which indicates that there was a lower ratio of unmethylated cytosines in the HFS-saline-offspring than in the ND-offspring, whereas there was a higher ratio in the HFS-GluOC-offspring. No methylated cytosines were found in XRE-3 in any of the groups.

We next measured the hepatic mRNA expression of epigenetic modifiers, such as the *de novo* DNA methyltransferases *Dnmt3a* and *Dnmt3b*, which catalyze the methylation reaction (the transfer of a

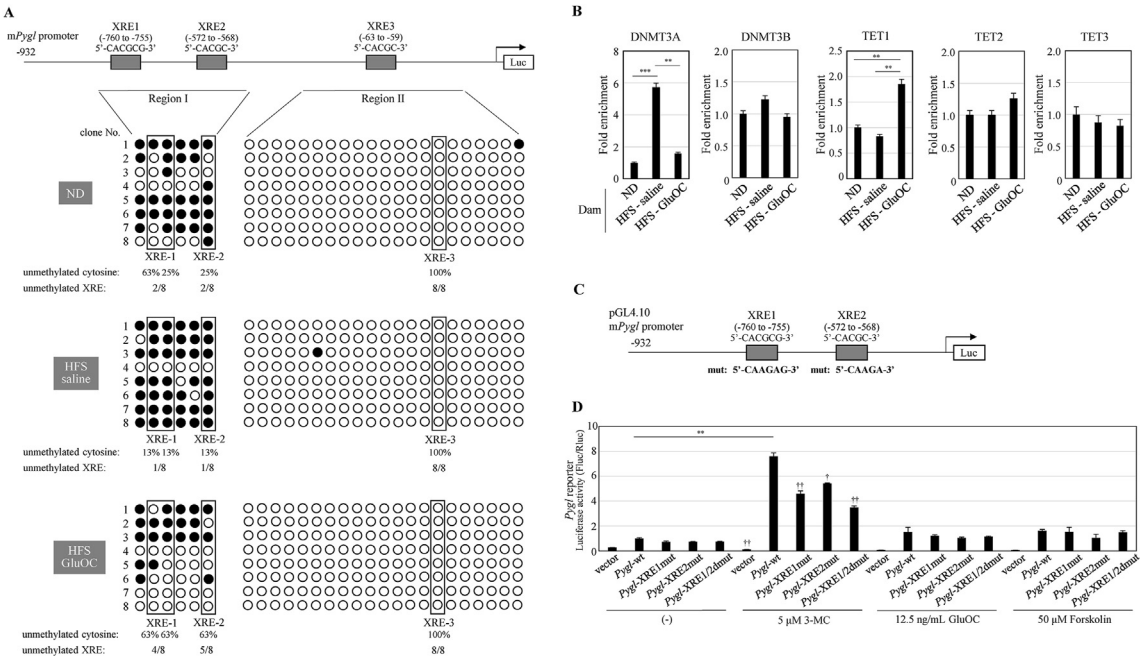

Figure 2: CpG methylation status in xenobiotic responsive elements (XREs) of the *Pygl* promoter is related to Pygl expression. (A) The methylation status of individual CpG sites in the *Pygl* upstream region in the P24 mouse liver was analyzed by bisulfite sequencing, focusing on Region I, which includes XRE-1 and XRE-2, and Region II, which includes XRE-3 (Supplementary Figure S2). The primers for the bisulfite sequencing assays are shown in the Supplementary Table 2. Circles indicate the positions of CpGs, and methylation status is depicted by open (unmethylated cytosine) and closed (methylated cytosine) circles for each CpG site. (B) Chromatin immunoprecipitation (ChIP) assays using chromatin purified from P24 liver and the indicated antibodies, followed by qPCR analysis for *Pygl*. The primers used for ChIP-qPCR are shown in Supplementary Table 3. Data are expressed as mean ± SEM of three independent experiments. Statistical analysis was performed using one-way ANOVA and Dunnett's *post-hoc* test. $^{**}P < 0.01$, $^{***}P < 0.001$. (C,D) Dual luciferase reporter assays using *Pygl* gene promoter constructs in mouse Hepa1c1c7 cells. (C) Schematic diagram showing the structure of the luciferase reporter pGL4.10. Mutant sequences are depicted in bold. (D) Reporter assay 24 h after transfection of each construct in the presence or absence of 5 μM 3-methylcholanthrene (MC), 12.5 ng/ml GluOC, and 50 μM forskolin. The dual-luciferase activity of three independent biological replicates was recorded for each assay. The *Renilla* luciferase activity of the pRL vector was used as the internal control. Fluc, firefly luciferase; Rluc, *Renilla* luciferase. Data are expressed as mean ± SEM. Statistical analysis was performed using one-way ANOVA and Dunnett's *post-hoc* test. $^{**}P < 0.01$. $^{\dagger}P < 0.05$ and $^{\dagger\dagger}P < 0.01$ *vs.* the 5 μM 3-MC-treated *Pygl*-wt transfectant.

methyl group to cytosine) [23—25], and the ten-eleven translocation (TET) methylcytosine dioxygenases, namely *Tet1*, *Tet2*, and *Tet3*, which catalyze the removal of methyl groups [26] in each of the groups. We found that the expression of *Dnmt3a* was lowest and that of *Tet1* was highest in the HFS-GluOC-offspring liver (Supplementary Figure S2). We then performed chromatin immunoprecipitation (ChIP)-qPCR assays of the expression of these epigenetic modifiers, because the expression levels of the mRNAs do not necessarily reflect the degree of binding of the encoded proteins to specific DNA loci [25]. Dnmt3a was found to be more highly bound to the *Pygl* promoter region, including XRE-1 and XRE-2, in the HFS-saline-offspring than in the ND-offspring, whereas the binding activity of Tet1 showed no difference between these groups. However, Tet1 was more highly bound to the hepatic *Pygl* promoter in HFS-GluOC-offspring than in the other two groups (Figure 2B). Considering that Dnmt3a and Tet1 act in complementary but competitive fashions in mice to mediate appropriate epigenetic and genetic regulation [27], the results of the ChIP-qPCR analysis were consistent with the frequency of CpG methylation at the XRE-1 and XRE-2 sites and the consequent mRNA expression of *Pygl* (Figures 1C and 2A).

We also performed dual-luciferase reporter assays using *Pygl* promoter constructs containing either wild-type (wt) or mutant (XRE-1 mutant, XRE-2 mutant, or XRE1/2 double mutant) expression vectors to determine whether these consensus sequences are involved in the regulation of *Pygl* transcription. Mouse hepatoma Hepa1c1c7 cells were transiently transfected with each luciferase reporter gene construct and incubated overnight with 5 μM 3-methylcholanthrene (3-MC), an Ahr agonist, to activate the Ahr-XRE axis [28], then luciferase activity was measured. When AhR forms a complex with ligands such as 3-MC, it translocates to the nucleus, where it heterodimerizes with aryl hydrocarbon nuclear translocator (Arnt), binds to XRE elements, and activates AhR-responsive genes [28]. The reporter assay showed that 3-MC induces *Pygl* promoter activity and that mutations in XRE-1 and XRE-2 partially inhibit this effect. Mutations in both XRE-1 and XRE-2 further reduced the promoter activity but could not completely prevent XRE-wt activity (Figure 2C and D). These findings imply that 3-MC stimulates *Pygl* promoter activity by activating the XRE-1 and XRE-2 sites. The transcriptional activity induced by 3-MC was not completely suppressed by any of the mutant constructs (Figure 2C and D), probably because of the existence of XRE-3 or another transcription factor. In contrast, the promoter was not activated by GluOC or forskolin, which has been reported to induce circadian Pygl expression [19] (Figure 2D).

3.3. Pygl expression in mouse liver is induced in an AhR-XRE-dependent manner

We next determined the effects of 3-MC at various concentrations on *Pygl* gene expression in Hepa1c1c7 cells, which are generally used for the analysis of the AhR function [29]. The mRNA expression of *Cyp1a1* [30] and *Cyp1a2* [31], well-known AhR-responsive genes, was significantly upregulated by 24 h of treatment with 3-MC in a dose-dependent manner (Figure 3A). *Pygl* mRNA expression was similarly

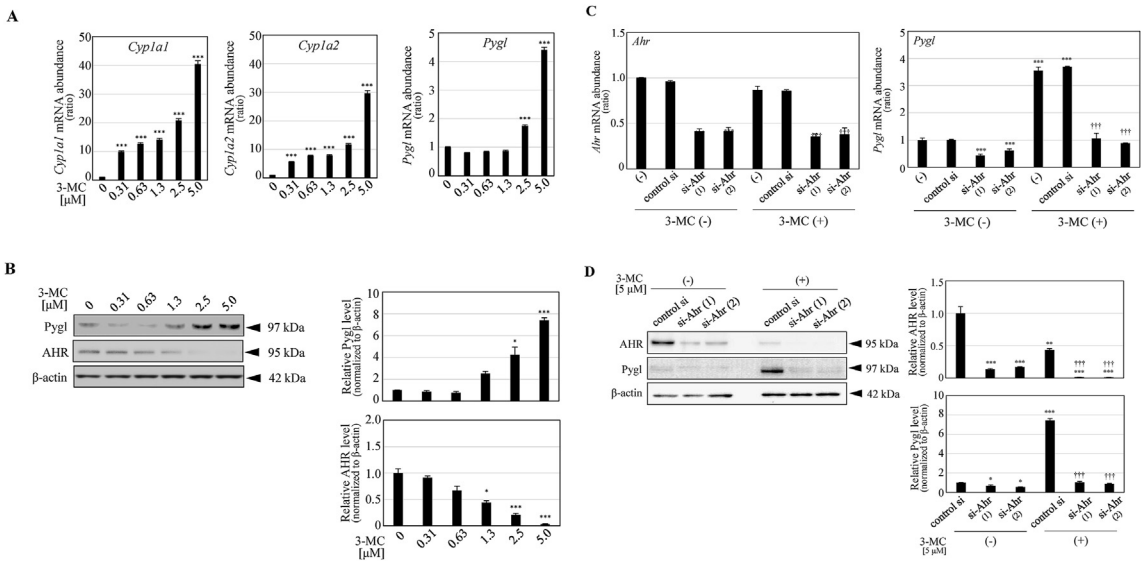

Figure 3: AHR is associated with *Pygl* expression in Hepa1c1c7 cells. (A) Quantitative RT-PCR analysis of *Cyp1a1*, *Cyp1a2*, and *Pygl* in Hepa1c1c7 cells treated with 3-MC (0—5.0 μM) for 24 h. *Actb* was used as the reference gene. (B) Left, immunoblot analysis of Pygl and AHR in Hepa1c1c7 cells treated with 3-MC (0—5.0 μM) for 24 h. Right, quantification of the blot (ratio of Pygl or Ahr expression to β-actin). (n = 3, pooled). Data are expressed as mean ± SEM of three independent experiments. Immunoblot shown is the typical one. Statistical analysis was performed using one-way ANOVA and Dunnett's *post-hoc* test. $^{*}P < 0.05$, $^{***}P < 0.001$. (C,D) mRNA (C) and protein (D) expression of Pygl and Ahr in Hepa1c1c7 cells transfected with either Ahr siRNA or control siRNA for 24 h, in the presence or absence of 5 μM 3-MC. The quantification of the immunoblots (ratio of Pygl or AHR to β-actin) is shown to the right of the immunoblot panels (n = 3, pooled). Data are expressed as mean ± SEM of three independent experiments. Statistical analysis was performed using one-way ANOVA and Dunnett's *post-hoc* test. $^{*}P < 0.05$, $^{**}P < 0.01$, $^{***}P < 0.001$ *vs.* 3-MC(−) control si; $^{\dagger\dagger\dagger}P < 0.001$ *vs.* 3-MC(+) control si.

increased by 2.5 and 5.0-μM concentrations of 3-MC, but to a relatively less extent than *Cyp1a1* and *Cyp1a2* expression. Immunoblot analysis also showed that Pygl protein expression was increased by the same concentrations of 3-MC (Figure 3B). Previous studies have shown that aryl hydrocarbon receptor (Ahr) protein is rapidly degraded when it binds ligands, such as 3-MC, *via* the ubiquitin-proteasome pathway [32—34]. The present results, showing that Ahr protein expression is dose-dependently reduced by 3-MC, are consistent with the previous findings (Figure 3B). The same experiments were then performed in the presence of lactacystin, an inhibitor of the ubiquitin-proteasome system. This inhibited Ahr degradation and caused a slight upregulation of Pygl expression (results not shown), consistent with its previously identified effects on the expression of Cyp1a1 and Cyp1b1 in mouse Hepa-1, and human RPE and MCF-7 cells [35,36]. To confirm the involvement of Ahr in the 3-MC-induced expression of Pygl *via* XRE, we determined the effects of siRNA-mediated knockdown of Ahr on Pygl expression. We first checked that Ahr expression was sufficiently reduced by the transfection of two types of siRNA targeting Ahr at both the mRNA and protein levels in the presence or absence of 3-MC (Figure 3C and D). The expression of Ahr protein in cells transfected with control siRNA after stimulation with 3-MC was lower, because of proteasomal degradation (Figure 3D). 3-MC increased Pygl expression at both the mRNA and protein levels (Figure 3C and D), but these increases did not occur in cells transfected with siRNA targeting Ahr (Figure 3C and D).

Notably, Ahr knockdown significantly reduced the constitutive expression of Pygl, in the absence of any stimulation (Figure 3C and D), indicating that an Ahr-dependent mechanism is involved in the physiological constitutive expression of Pygl in mouse hepatocytes. However, little is known regarding the physiological roles of endogenous Ahr ligand [37—39].

We next determined whether choline bitartrate (CB) or tert-butylhydroquinone (TBHQ), chemical substances present in the HFS diet, are Ahr ligands because the known exogenous Ahr ligands that act on XRE regions are chemical compounds such as polycyclic aromatic hydrocarbons, polyhalogenated hydrocarbons, and dibenzofurans [40]. However, neither of these compounds induced the expression of *Cyp1a1*, *Cyp1a2*, or *Pygl*, except an induction of *Cyp1a2* by TBHQ (Supplementary Figure S3), which implies that these dietary compounds are not Ahr activators. Overall, these results indicate that the lower Pygl expression in the livers of HFS-saline-offspring (Figure 1B and C) can be attributed to methylation of the XRE-1 and -2 regions of the *Pygl* promoter (Figure 2A—D) and that this might be a cause of the previously observed aberrant metabolism in mature HFS-saline-offspring [14].

3.4. GluOC administration during pregnancy affects OC expression and subsequent Pygl expression in the offspring

Next, we determined whether the *Pygl* expression shown in Figure 1C, measured using qRT-PCR, was reflected in protein expression, determined using immunohistochemical analysis. Immunostaining for Pygl appeared to be lower in the livers of HFS-saline-offspring than in those of the ND-offspring (Figure 4A), but more intense staining was evident in HFS-GluOC-offspring liver than in ND-offspring liver (Figure 4A). This finding was confirmed using immunoblot analysis (Figure 4B).

Previous studies showed the expression of OC mRNA in various organs and tissues, including the liver, in addition to bone [5], and that maternal OC could cross the placenta [41]. Therefore, we performed immunohistochemical analysis to characterize OC expression in the livers of offspring at P24. We found OC protein expression in the liver, which was more abundant in the livers of HFS-GluOC-offspring than in the livers of mice in the other two groups (Figure 4A), despite the dams not having been administered GluOC for the preceding 24 days, during lactation. Immunoblotting of liver extracts also confirmed that OC protein was expressed at much higher levels in the livers of HFS-

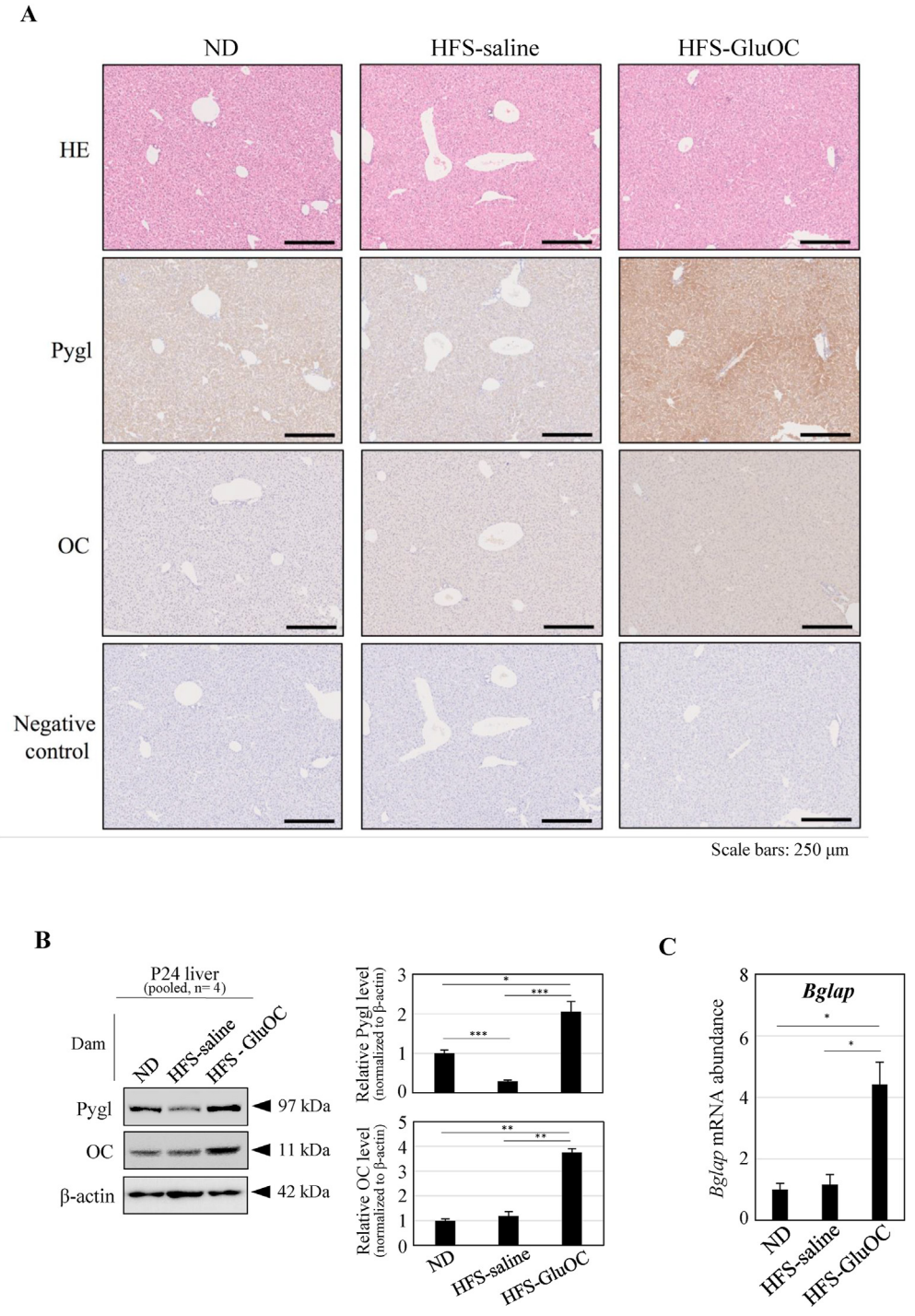

Figure 4: OC expression is high in the livers of P24 offspring of HFS-GluOC dams. (A) Hematoxylin and eosin staining and immunohistochemistry for Pygl and OC in P24 mouse livers from the ND-, HFS-saline-, and HFS-GluOC-offspring groups under non-fasting conditions. Scale bars are 250 μm. Typical staining is shown from more than 10 specimens. (B) Left, immunoblot analysis of Pygl and OC. Right, quantification of the blots (ratio of Pygl or OC to β-actin). (n = 4, pooled). (C) Quantitative RT-qPCR analysis of *Bglap* in P24 mouse livers from each group (n = 3). *Actb* was used as the reference gene. Data are expressed as mean ± SEM of 3–4 independent experiments. Statistical analysis was performed using one-way ANOVA and Dunnett's *post-hoc* test. $^{*}P < 0.05$, $^{**}P < 0.01$, and $^{***}P < 0.001$.

GluOC-offspring than in those of the other two groups (Figure 4B), and qRT-PCR analysis showed similar patterns of OC expression among the three groups as the immunohistochemical and immunoblotting measurements (Figure 4C). The OC protein found in the mouse liver was predominantly 11 kDa in size, probably representing a pre-pro form of OC (Figure 4B) [42]. Next, to determine whether the expression of OC in the liver is regulated by DNA methylation, we analyzed the methylation status of the *Bglap* (an OC family gene) promoter in the liver of P24 offspring using bisulfite genomic sequencing in the three groups, as for *Pygl* (Figure 2A). Consistent patterns of methylation were not found

among the three groups; more unmethylated CpGs were found in the HFS-offspring than in the ND-offspring in Region I, whereas fewer unmethylated CpGs were reported only in the HFS-GluOC-offspring in Region II, which implies that OC expression is not regulated by DNA methylation in the gene promoter region (Supplementary Figure S4A and B).

The significant expression of Pygl in HFS-GluOC-offspring than in the other two groups may be explained by less methylation of the *Pygl* promoter; the higher expression of OC suggests a relationship between OC and Pygl expression. Therefore, we next determined the effects of GluOC treatment in Hepa1c1c7 cells and found dose-dependent increases in Pygl expression and that of OC itself at both the mRNA and protein levels (Figure 5A and B). The OC produced in Hepa1c1c7 cells was also predominantly of 11 kDa molecular mass, which likely represents a pre-pro-form of OC (Figure 5B) that may not be secreted. Therefore, we stimulated Hepa1c1c7 cells with forskolin, which induces cAMP accumulation and activates the OC promoter [43–45]. Forskolin caused an increase in OC in both its GlaOC and GluOC forms of approximately 2-fold and 8-fold, respectively, and approximately 10% and 5% of the GlaOC and GluOC, respectively, were detected outside the cells (Figure 5C), which implies that at least some of the OC was secreted and could therefore have extracellular effects. The molecular mass of the secreted OC was approximately 5 kDa, which probably represents a mature form (Supplementary Figure S5). We then determined the effect of knocking down the expression of GPRC6A, a putative receptor for GluOC, on the OC-induced expression of Pygl and OC itself. The siRNA-induced knockdown of GPRC6A reduced the expression of both Pygl and OC (Figure 5D). Given that the luciferase reporter assays revealed that neither 50 μM forskolin, nor 12.5 ng/ml GluOC, promotes the transcriptional activity of *Pygl via* XREs (Figure 2D), these results suggest that the much higher Pygl expression in the livers of HFS-GluOC-offspring at P24 might result from feed-forward induction of OC synthesis, which might be induced by exposure of the fetus to transplacentally-derived maternal GluOC, in addition to the effects of DNA hypomethylation induced by GluOC activation of XRE elements in the *Pygl* promoter. This feed-forward mechanism appears to have long-term effects because the same patterns of expression of Pygl and OC in the three groups of mice that identified at P24 were found to be present in the livers of offspring at P95, although the differences between the groups were significant at a subsequent time point (Supplementary Figure S6A). The P95 liver samples used for this analysis (Supplementary Figure S6A and B) were those prepared in paraffin blocks during our previous study conducted more than 6 years previously [14] when we were unaware of the relationship between OC and Pygl and glycogen.

To explore the mechanisms whereby GluOC regulates Pygl and OC expression in Hepa1c1c7 cells, we assessed the roles of cyclic adenosine monophosphate (cAMP)-responsive element-binding protein H (CREBH) and activating transcription factor 4 (ATF4) using siRNA technology. The administration of GluOC increased the expression of

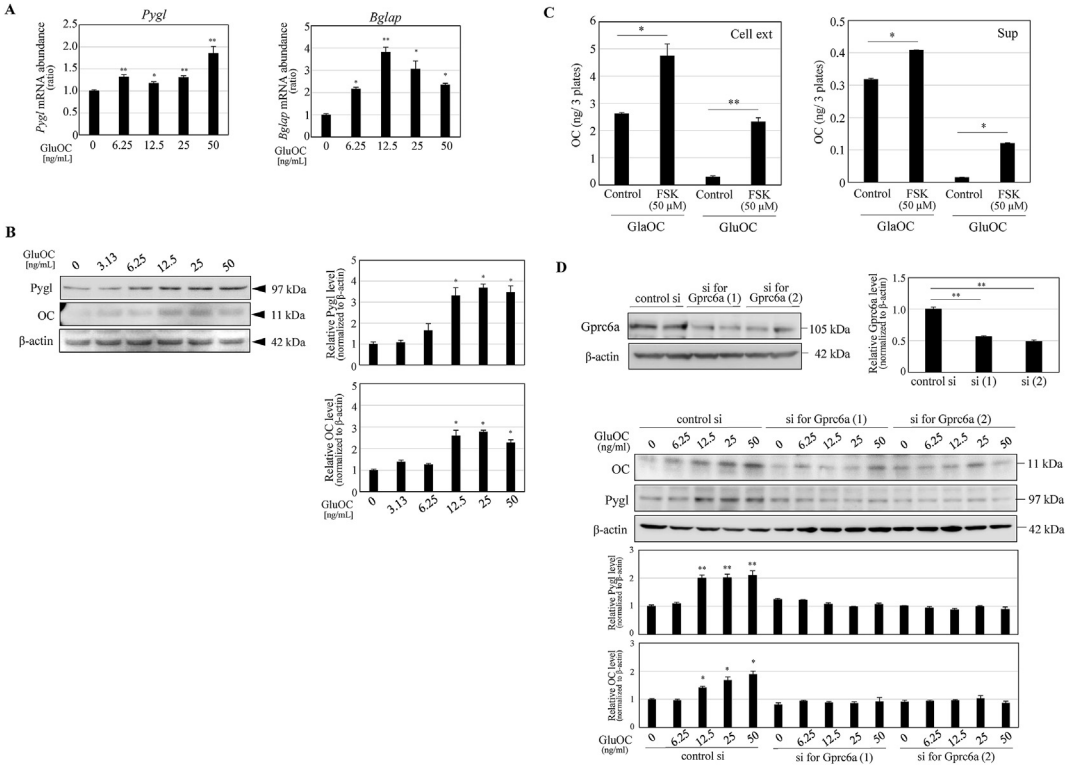

Figure 5: OC expression is related to Pygl expression in mouse Hepa1c1c7 cells. (A, B) mRNA (A) and protein (B) expression of Pygl and OC in Hepa1c1c7 cells treated with GluOC (0–50 ng/ml) for 24 h. Levels of *Actb*/β-actin were determined as internal controls. (B) Left, immunoblot analysis. Right, quantification of the blot (ratio of Pygl or OC to β-actin). (C) ELISA assays of GlaOC and GluOC in Hepa1c1c7 cell extracts (left) and supernatants (right) after 50 μM forskolin treatment for 24 h. Cells (7.5×10^6) were pre-cultured in 150 mm plates overnight, then incubated with 50 μM forskolin or DMSO for 24 h. The supernatants were lyophilized and dissolved in a small quantity of water, dialyzed against water, and then assayed for Gla- or GluOC by ELISA. (D) Top: knockdown of Gprc6A by siRNA; Middle: expression of OC and Pygl in Hepa1c1c7 cells transfected with Gprc6a siRNA or control siRNA for 24 h in the presence of GluOC (0–50 ng/ml); Bottom: Quantification of the immunoblots (ratio of Pygl or AHR to β-actin). Data are expressed as mean ± SEM of three independent experiments. The blot shown is the typical one. Statistical analysis was performed using one-way ANOVA and Dunnett's *post-hoc* test. $^*P < 0.05$, $^{**}P < 0.01$, and $^{***}P < 0.001$.

CREBH despite CREBH siRNA treatment, as shown in the top lane in Supplementary Figure S7A, although the corresponding mRNA was less abundant, as expected, which suggests that GluOC stimulates the translation of CREBH. Pygl and OC were expressed in accordance with the abundance of CREBH protein in cells treated with GluOC, but they were expressed at similar levels in siRNA-treated cells that had not been treated with GluOC (Supplementary Figure S7A). In contrast, ATF4 expression was further reduced by GluOC application at both the protein and mRNA levels, and Pygl and OC expression was consistent with this (Supplementary Figure S7B). Conversely, the activation of CREBH, indicated by the production of the cleaved form of CREBH in response to endoplasmic reticulum stress-induced by tunicamycin [46], increased the expression of Pygl and OC in a dose-dependent manner (Supplementary Figure S7C). These data collectively imply that GluOC activates GPRC6A, which is followed by the activation of CREBH and ATF4, and consequent increases in the expression of Pygl and OC itself.

3.5. The regulation of Pygl by maternal nutrition in mouse liver is physiologically relevant

We next determined whether the effects of maternal diet on the hepatic Pygl expression in mouse offspring and of GluOC administration are physiologically relevant. The fresh liver was obtained from non-fasting mice for the measurement of Pygl activity, and that of the HFS-saline-offspring was reduced to about half of that of the ND-offspring, whereas that of the HFS-GluOC-offspring was similar (Figure 6A). In addition, the hepatic glycogen content inversely correlated with the Pygl activity (Figure 6B), and periodic acid-Schiff (PAS) staining showed obvious glycogen accumulation in the livers of HFS-saline-offspring, compared with the other two groups, and this staining disappeared after amylase treatment of the tissue sections (Figure 6G). Moreover, the hepatic free glucose concentration also inversely correlated with the amount of hepatic glycogen (Figure 6C), and the HFS-saline offspring had the lowest non-fasting blood glucose concentrations (Figure 6D).

We also examined periodic acid-Schiff (PAS)-stained liver sections from P95 offspring. Staining in the liver, indicative of glycogen accumulation, was most evident in HFS-saline-offspring fed an ND after weaning than in the other groups, and this disappeared after amylase treatment, as for the staining of the P24 sections. However, it was difficult to observe glycogen accumulation in HFS-fed offspring at P95 because of the large number of lipid droplets present (Supplementary Figure S6B). We also confirmed our previous observation [14] that there was a lower accumulation of lipid droplets in the liver of P95 offspring from HFS-GluOC dams than in those from HFS-saline dams. We previously reported that the P95 offspring from HFS-saline dams exhibited a metabolic disorder, characterized by higher body weight, glucose intolerance assessed using intraperitoneal glucose tolerance test (IPGTT), insulin resistance (assessed using ITT), ectopic lipid accumulation in the liver, greater gonadal fat mass, enlarged adipocytes, macrophage infiltration into fat forming crown-like structures and higher expression of proinflammatory cytokines, such as IL-6, TNFα, CD11c, MCP-1 and F4/80 in adipose, all of which were ameliorated in the offspring of HFS-GluOC dams [14].

A recent study showed that sucrose feeding causes triglyceride (TG) accumulation in the liver [47]; therefore, we also measured the hepatic and serum concentrations of TG and found that TG was present at significantly higher concentrations in the liver (Figure 6E), but not in the serum (Figure 6F), of HFS-saline-offspring at P24, compared with the other two groups, as described in our previous study [14]. Finally, mice in the HFS-saline-offspring group had significantly higher body and wet liver masses than the other two groups (Figure 6H and I).

4. DISCUSSION

In our previous study, we demonstrated that feeding an HFS diet during gestation results in higher body mass gain and more severe metabolic disorders in the offspring fed HFS after weaning; and that oral administration of GluOC to the mothers during gestation largely prevents the obesity and metabolic abnormalities in their offspring [14]. Given that maternal nutrition and GluOC administration during gestation affect the offspring during and after maturation, we hypothesized that an *in utero* inherited epigenetic mechanism might at least in part determine the phenotypes of the offspring. Therefore, in the present study, we attempted to identify the gene(s) responsible for the metabolic disorders by performing a comprehensive DNA methylation analysis of the liver of the offspring at P24. Thus, we found that the expression of *Pygl*, which is involved in energy homeostasis, is modified by both the maternal diet and GluOC administration. Specifically, Pygl expression and activation in the offspring were reduced by maternal HFS-feeding during gestation, resulting in excessive hepatic glycogen accumulation and hepatomegaly, similar to that of *Pygl*-deficient mice [20]. The mutant mice also had low random serum glucose concentrations and high hepatic inflammatory cytokine concentrations, such as those of monocyte chemoattractant protein (MCP)-1, interleukin (IL)-6, and tumor necrosis factor (TNF)-α [20], consistent with the findings in HFS-saline-offspring mice in the current as well as our previous study [14]. The low expression and activity of Pygl were prevented by the administration of GluOC during pregnancy, and the levels were higher than in the control mice, as discussed below.

Liver glycogen is an energy source for the whole body, being used to replenish blood glucose during fasting through glycogenolysis. Long-term fasting depletes liver glycogen, such that TG from adipose tissue must be utilized, involving its hydrolysis to glycerol and fatty acids, followed by β-oxidation of the latter [48]. A recent study demonstrated that this shift in energy source from hepatic glycogen to adipose tissue TG involves Pygl-mediated glycogen depletion and liver-brain-adipose neurocircuitry [48]. Thus, Pygl activity is linked to the use of adipose tissue TG. In metabolic disorders, such as obesity, TG accumulates in adipose tissue but is also deposited ectopically in the liver, which is strongly associated with the development of insulin resistance [49]. Therefore, the promotion of TG catabolism and/or the inhibition of its synthesis, may ameliorate such disorders and their clinical consequences. In our previous study, feeding of an HFS diet after weaning induced obesity in mice, as shown by heavier perigonadal white adipose tissue depots, abnormal energy metabolism, and insulin resistance in P95 female HFS-saline-offspring, in comparison to ND-offspring [14]. In addition, both glycogen and TG accumulated in the livers of the mice. These results suggest that a decrease in Pygl expression and activity, perhaps because of DNA hypermethylation, might explain the subsequent suppression of adipose lipolysis in female HFS-saline-offspring, which results in obesity. Of the various types of epigenomic modification, DNA methylation is known to be preserved and inherited over more than one generation [3]. Therefore, it is reasonable to believe that the DNA methylation status of the *Pygl* promoter region would be imprinted during the fetal period, or by P24 at the latest. Furthermore, because DNA methylation is known to be conserved between mouse and human [50], and mouse and human Pygl proteins share 94% sequence homology [20], the same mechanism may exist in humans.

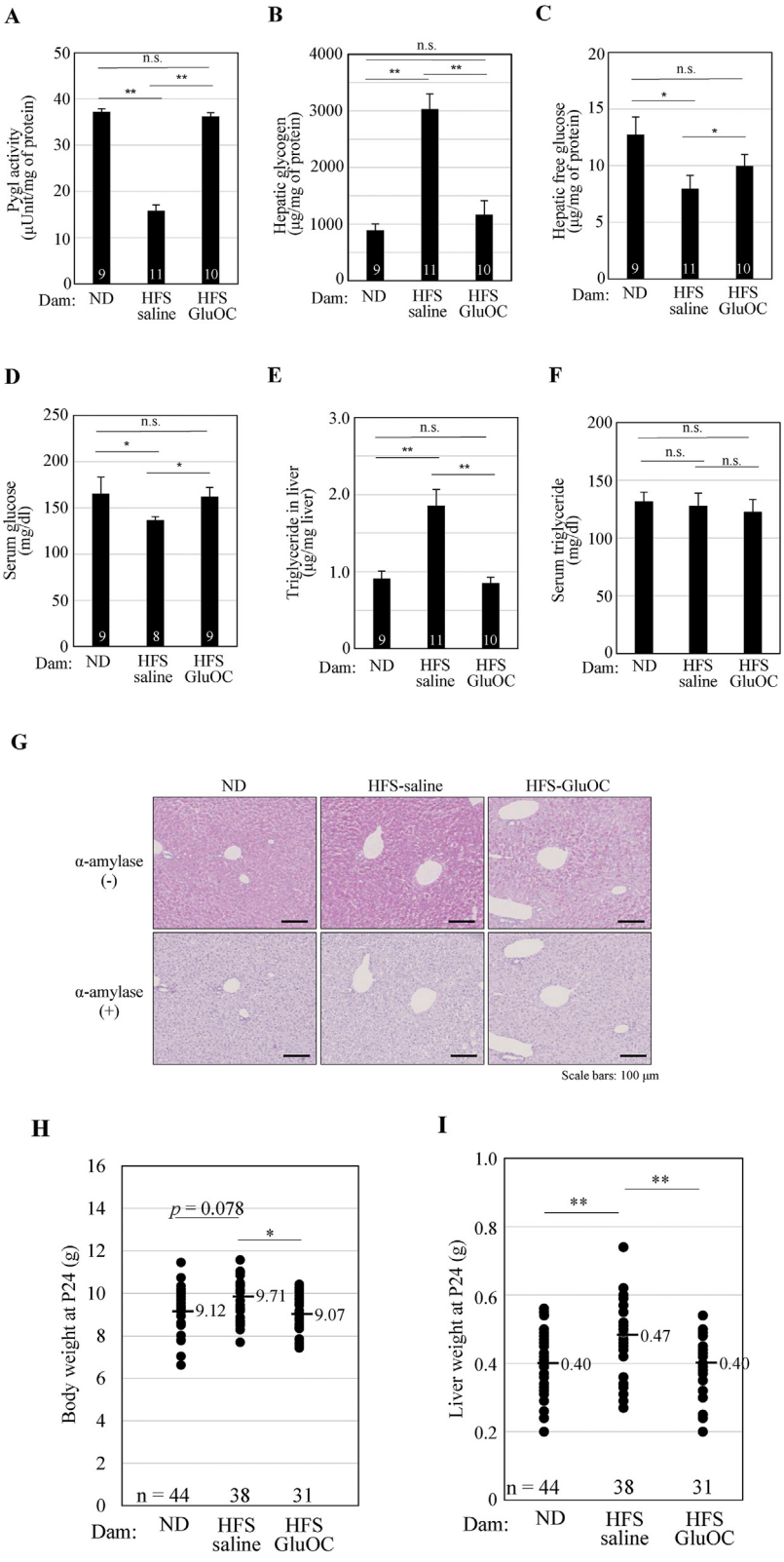

Figure 6: Assessment of the metabolism of the P24 mice. Biological assays for (A) Pygl activity, (B) hepatic glycogen, (C) hepatic free glucose, (D) serum glucose, and (E) hepatic and (F) serum triglyceride. The numbers in the columns are the number of samples measured. Data are expressed as mean ± SEM. (G) PAS staining of P24 liver from female offspring in each group, with or without α-amylase treatment, using consecutive tissue sections. Typical staining is shown from more than 10 specimens. (H, I) Body (H) and liver (I) mass of P24 offspring. The numbers in the columns are the number of samples measured. The horizontal bar indicates the mean with the value. Statistical analysis was performed using one-way ANOVA and Dunnett's *post-hoc* test. $*P < 0.05$ and $**P < 0.01$.

An analysis of the enzymes responsible for DNA methylation by qRT-PCR and ChIP-qPCR assay revealed that Dnmt3a and Tet1 were affected by maternal nutrition and GluOC administration. Dnmt3a was found to bind to XREs in large quantities, without showing any difference in mRNA expression, and hepatic Tet1 was unaffected by maternal HFS nutrition at P24, which would have resulted in the hypermethylation of XREs. The administration of GluOC during pregnancy caused a decrease in the mRNA expression and the binding of Dnmt3a to XREs, whereas it increased both the mRNA expression and binding of Tet1, which together resulted in lower methylation of XREs, thereby antagonizing the effect of the maternal HFS diet. However, the molecular mechanisms involved in the effects of HFS diet-feeding and GluOC administration during pregnancy on the mRNA expression of and XRE-binding by Dnmt3a and Tet1 require further elucidation.

Cyclic adenosine monophosphate-response element-binding protein H (CREBH has been reported to be involved in the circadian expression of *Pygl* in fasting mice [19]. However, in the present study, the methylation status of CREBH binding sites in the *Pygl* promoter was not modified by HFS-feeding in mouse liver. Rather, we have shown that Ahr-XREs are required for both constitutive and inducible Pygl expression in mouse liver, where a yet-to-be-identified endogenous Ahr ligand has its effects, and that the methylation status of these elements in *Pygl* promoter is modulated by *in utero* nutrition, with effects that can persist into adulthood. Whereas a relationship between Ahr and Pygl has been shown in previous studies [51,52], to our knowledge, the present study is the first to show that the Ahr activated by an exogenous ligand, 3-MC, binds to XREs and induces the expression of a target gene, *Pygl*. However, the endogenous ligands for Ahr that would promote *Pygl* expression have not been definitively identified. Several endogenous ligands and activators of Ahr have been reported, but the specific mechanism of its activation *in vivo* has not been characterized [37,39,40,53] yet, and Ahr may also be activated independently of a ligand [54]. Silencing of Ahr using siRNA markedly reduced the expression of Pygl in hepatocytes in the absence of any specific stimulation, which suggests that constitutive activation of Ahr-XREs is sufficient to cause the expression of Pygl and to maintain blood glucose concentration during fasting.

We found that maternal GluOC administration during gestation increased hepatic Pygl expression to a level that was higher than that of the offspring from ND-fed dams. This might be attributable to hypomethylation of the XRE region causing higher Pygl expression, because of lower expression of Dnmt3a and higher expression of Tet1. In addition, maternal GluOC administration during gestation induced higher OC expression in the offspring liver at P24. The circadian rhythms of Pygl expression [19] and serum OC concentration [55] are similar in mice, with peaks between 09:00 a.m. and 12:00 a.m.. Furthermore, circadian Pygl expression is reported to be dependent on regulation by CREBH during fasting [19,56] and GluOC induces cAMP production both in adipocytes [57] and hepatocytes (data not shown). Moreover, cAMP has been reported to directly induce Ahr activation [40] and OC promoter activity is promoted by cAMP accumulation [43–45]. These results indicate an association between Pygl expression and OC in the liver. The present experiments using Hepa1c1c7 cells revealed that GluOC induces intracellular cAMP accumulation, which activates CREBH and ATF4, resulting in the upregulation of GluOC itself and Pygl, but this is inhibited by silencing GPRC6A, a putative receptor for GluOC. Furthermore, the GluOC produced in hepatocytes is in part secreted in the mature form, which implies that GluOC derived from hepatocytes may activate GPRC6A to induce the expression of Pygl and that of OC itself, in a feed-forward loop in an autocrine and/or paracrine manner. GluOC may pass through the placenta to induce this feed-forward loop in the liver of the fetus, and the effects appear to last in the liver until P24 and P95. Considering that Pygl upregulation has also been shown to be induced by an increase in intracellular cAMP concentration [19,56,58], we believe that the high Pygl expression in the livers of HFS-GluOC-offspring is the result not only of *Pygl* hypomethylation, but also of an OC-mediated process, which together reduce glycogen accumulation in HFS-GluOC-offspring *versus* HFS-saline-offspring. Pi et al. reported that GPRC6A expression in *Hepa1c1c7* cells is important for glucose production and that loss of *Gprc6a* function in hepatocytes results in alterations in the expression of genes that are involved in glycogen metabolism [59]; Zhang et al., using a liver-specific Gprc6a knockout mouse showed that Gprc6a directly mediates the effects of GluOC in the liver [60].

In the present study, eight genes other than *Pygl* are also shown to be expressed at lower levels in the livers of HFS-saline-offspring than in those of ND-offspring, probably because of hypermethylation of their promoter regions. These differences in gene expression might also influence the phenotype of the HFS-offspring after maturation. For example, abnormal TG accumulation was present in the livers of HFS-saline-offspring, which might be attributable to the downregulation of *Apob*, because of hypermethylation of its promoter region in the HFS-offspring liver. An isoform of ApoB synthesized in hepatocytes is ApoB-100, which is a major structural component of very-low-density lipoprotein (VLDL) and low-density lipoprotein, forming VLDL with TG and cholesterol, and this is secreted into the circulation [61]. A significant decrease in ApoB-100 expression might reduce the release of hepatic TG into the circulation, resulting in TG accumulation in the liver. The expression of genes, other than *Pygl* and *Apob*, was also altered by HFS; few genes were further downregulated in response to gestational GluOC administration, which implies that they might share responsibility for the metabolic phenotype of the offspring at P24 in the present study and P95 in the previous study [14].

We conclude that *Pygl* expression is epigenetically suppressed through DNA hypermethylation *in utero* secondary to excessive maternal sucrose and fat consumption, and this imprinting effect can persist in the offspring into adulthood when fat utilization is reduced as a result of aberrant glycogen metabolism. Additionally, maternal GluOC administration prevents abnormal energy metabolism in the offspring by improving Pygl expression and activity. Thus, Pygl and GluOC are important for the developmental imprinting of energy metabolism and appropriate expression and activity levels are required for efficient fat utilization in subsequent generations. Our results confirm that factors determined by the *in utero* environment, which have been described using the term "body constitution" [62,63], may be an important cause of lifestyle-related diseases, such as obesity.

AUTHORS' CONTRIBUTIONS

T.K—Y. designed and performed the experiments, analyzed the data, and wrote the manuscript. E.Y., T.N., A.M., S.K., Y.H., K.O., and A.Y. performed the experiments and analyzed the data. Y.H., S.N. and E.J. evaluated the data and participated in preparing the manuscript. M.H. supervised the entire project, provided suggestions for experiments, analyzed data, and wrote the manuscript.

ACKNOWLEDGMENTS

The authors thank Professor Manabu Nakashima, who has retired from the Department of Immunological and Molecular Pharmacology, Faculty of Pharmaceutical Sciences, Fukuoka University, Japan, for helpful discussions; Dr. Atsushi Doi, Dr. Hiroko Hagiwara, and Dr. Kaori Yasuda (Cell Innovator Co., Ltd., Fukuoka,

Japan) for assistance with the sequencing analysis and useful discussion; and Hikari Takeshima and Mayu Seida, undergraduate students in the Department of Biomedical Science, Kyushu University School of Medicine, for technical assistance. We also appreciate the technical assistance provided by the Research Support Center, Research Center for Human Disease Modeling, Kyushu University Graduate School of Medical Sciences. This work was supported by the Japan Society for the Promotion of Science (KAKENHI grants JP17H01595 and JP20H03854 to M.H., JP19K10052 to T.K.-Y., JP18K09521 to A.M., and JP19K10269 to A.Y.), the Shinnihon Foundation of Advanced Medical Treatment Research, the Danone Institute of Japan Foundation, Japan, and the Mishima Kaiun Memorial Foundation. We also thank Mark Cleasby, Ph.D. from Edanz (https://jp.edanz.com/ac) for editing a draft of this manuscript.

CONFLICT OF INTEREST

The authors declare no competing interests.

APPENDIX A. SUPPLEMENTARY DATA

Supplementary data to this article can be found online at https://doi.org/10.1016/j.molmet.2021.101360.

REFERENCES

[1] NCD Countdown 2030 collaborators, 2018. NCD Countdown 2030: worldwide trends in non-communicable disease mortality and progress towards Sustainable Development Goal target 3.4. Lancet 392(10152):1072–1088.

[2] McKerracher, L., Moffat, T., Barker, M., Williams, D., Sloboda, D.M., 2019. Translating the Developmental Origins of Health and Disease concept to improve the nutritional environment for our next generations: a call for a reflexive, positive, multi-level approach. Journal of Development Origin of Health Disease 10(4):420–428.

[3] van Otterdijk, S.D., Michels, K.B., 2016. Transgenerational epigenetic inheritance in mammals: how good is the evidence? The FASEB Journal 30(7):2457–2465.

[4] Messerschmidt, D.M., Knowles, B.B., Solter, D., 2014. DNA methylation dynamics during epigenetic reprogramming in the germline and preimplantation embryos. Genes & Development 28(8):812–828.

[5] Fleet, J.C., Hock, J.M., 1994. Identification of osteocalcin mRNA in nonosteoid tissue of rats and humans by reverse transcription-polymerase chain reaction. Journal of Bone and Mineral Research 9(10):1565–1573.

[6] Ferron, M., Hinoi, E., Karsenty, G., Ducy, P., 2008. Osteocalcin differentially regulates beta cell and adipocyte gene expression and affects the development of metabolic diseases in wild-type mice. Proceedings of the National Academy of Sciences of the United States of America 105(13):5266–5270.

[7] Ferron, M., Wei, J., Yoshizawa, T., Del Fattore, A., DePinho, R.A., Teti, A., et al., 2010. Insulin signaling in osteoblasts integrates bone remodeling and energy metabolism. Cell 142(2):296–308.

[8] Fulzele, K., Riddle, R.C., DiGirolamo, D.J., Cao, X., Wan, C., Chen, D., et al., 2010. Insulin receptor signaling in osteoblasts regulates postnatal bone acquisition and body composition. Cell 142(2):309–319.

[9] Lee, N.K., Sowa, H., Hinoi, E., Ferron, M., Ahn, J.D., Confavreux, C., et al., 2007. Endocrine regulation of energy metabolism by the skeleton. Cell 130(3):456–469.

[10] Mizokami, A., Mukai, S., Gao, J., Kawakubo-Yasukochi, T., Otani, T., Takeuchi, H., et al., 2020. GLP-1 signaling is required for improvement of glucose tolerance by osteocalcin. Journal of Endocrinology 244(2):285–296.

[11] Mizokami, A., Yasutake, Y., Higashi, S., Kawakubo-Yasukochi, T., Chishaki, S., Takahashi, I., et al., 2014. Oral administration of osteocalcin improves glucose utilization by stimulating glucagon-like peptide-1 secretion. Bone 69:68–79.

[12] Otani, T., Mizokami, A., Hayashi, Y., Gao, J., Mori, Y., Nakamura, S., et al., 2015. Signaling pathway for adiponectin expression in adipocytes by osteocalcin. Cellular Signalling 27(3):532–544.

[13] Pi, M., Nishimoto, S.K., Quarles, L.D., 2017. GPRC6A: jack of all metabolism (or master of none). Molecular Metabolism 6(2):185–193.

[14] Kawakubo-Yasukochi, T., Kondo, A., Mizokami, A., Hayashi, Y., Chishaki, S., Nakamura, S., et al., 2016. Maternal oral administration of osteocalcin protects offspring from metabolic impairment in adulthood. Obesity 24(4):895–907.

[15] Hankinson, O., 1981. Evidence that Benzo(a) pyrene-resistant, aryl hydrocarbon hydroxylase-deficient variants of mouse hepatoma line, Hepa-1, are mutational in origin. Somatic Cell Genetics 7(4):373–388.

[16] Bolger, A.M., Lohse, M., Usadel, B., 2014. Trimmomatic: a flexible trimmer for Illumina sequence data. Bioinformatics 30(15):2114–2120.

[17] Xi, Y., Li, W., 2009. BSMAP: whole genome bisulfite sequence MAPping program. BMC Bioinformatics 10:232.

[18] Li, R., Li, Y., Kristiansen, K., Wang, J., 2008. SOAP: short oligonucleotide alignment program. Bioinformatics 24(5):713–714.

[19] Kim, H., Zheng, Z., Walker, P.D., Kapatos, G., Zhang, K., 2017. CREBH maintains circadian glucose homeostasis by regulating hepatic glycogenolysis and gluconeogenesis. Molecular and Cellular Biology 37(14):e00048, 17.

[20] Wilson, L.H., Cho, J.H., Estrella, A., Smyth, J.A., Wu, R., Chengsupanimit, T., et al., 2019. Liver glycogen phosphorylase deficiency leads to profibrogenic phenotype in a murine model of glycogen storage disease type VI. Hepatology Communications 3(11):1544–1555.

[21] Bell, J.T., Pai, A.A., Pickrell, J.K., Gaffney, D.J., Pique-Regi, R., Degner, J.F., et al., 2011. DNA methylation patterns associate with genetic and gene expression variation in HapMap cell lines. Genome Biology 12(1):R10.

[22] Huang, D.W., Sherman, B.T., Lempicki, R.A., 2009. Systematic and integrative analysis of large gene lists using DAVID bioinformatics resources. Nature Protocols 4(1):44–57.

[23] Jones, P.A., Liang, G., 2009. Liang, Rethinking how DNA methylation patterns are maintained. Nature Reviews Genetics 10(11):805–811.

[24] Okano, M., Bell, D.W., Haber, D.A., Li, E., 1999. DNA methyltransferases Dnmt3a and Dnmt3b are essential for de novo methylation and mammalian development. Cell 99(3):247–257.

[25] Rinaldi, L., Datta, D., Serrat, J., Morey, L., Solanas, G., Avgustinova, A., et al., 2016. Dnmt3a and Dnmt3b associate with enhancers to regulate human epidermal stem cell homeostasis. Cell Stem Cell 19(4):491–501.

[26] Tahiliani, M., Koh, K.P., Shen, Y., Pastor, W.A., Bandukwala, H., Brudno, Y., et al., 2009. Conversion of 5-methylcytosine to 5-hydroxymethylcytosine in mammalian DNA by MLL partner TET1. Science 324(5929):930–935.

[27] Gu, T., Lin, X., Cullen, S.M., Luo, M., Jeong, M., Estecio, M., et al., 2018. DNMT3A and TET1 cooperate to regulate promoter epigenetic landscapes in mouse embryonic stem cells. Genome Biology 19(1):88.

[28] Edamitsu, T., Taguchi, K., Kobayashi, E.H., Okuyama, R., Yamamoto, M., 2019. Aryl hydrocarbon receptor directly regulates artemin gene expression. Molecular and Cellular Biology 39(20):e00190, 19.

[29] Kim, Y.C., Seok, S., Byun, S., Kong, B., Zhang, Y., Guo, G., et al., 2018. AhR and SHP regulate phosphatidylcholine and S-adenosylmethionine levels in the one-carbon cycle. Nature Communications 9(1):540.

[30] Whitlock Jr., J.P., Okino, S.T., Dong, L., Ko, H.P., Clarke-Katzenberg, R., Ma, Q., et al., 1996. Cytochromes P450 5: induction of cytochrome P4501A1: a model for analyzing mammalian gene transcription. The FASEB Journal 10(8):809–818.

[31] Larsen, M.C., Angus, W.G., Brake, P.B., Eltom, S.E., Sukow, K.A., Jefcoate, C.R., 1998. Characterization of CYP1B1 and CYP1A1 expression in human mammary epithelial cells: role of the aryl hydrocarbon receptor in polycyclic aromatic hydrocarbon metabolism. Cancer Research 58(11):2366–2374.

[32] Giannone, J.V., Li, W., Probst, M., Okey, A.B., 1998. Prolonged depletion of AH receptor without alteration of receptor mRNA levels after treatment of cells in

culture with 2,3,7,8-tetrachlorodibenzo-p-dioxin. Biochemical Pharmacology 55(4):489—497.

[33] Ma, Q., Baldwin, K.T., 2000. 2,3,7,8-tetrachlorodibenzo-p-dioxin-induced degradation of aryl hydrocarbon receptor (AhR) by the ubiquitin-proteasome pathway. Role of the transcription activaton and DNA binding of AhR. Journal of Biological Chemistry 275(12):8432—8438.

[34] Pollenz, R.S., 2002. The mechanism of AH receptor protein down-regulation (degradation) and its impact on AH receptor-mediated gene regulation. Chemico-Biological Interactions 141(1—2):41—61.

[35] Choi, H., Chun, Y.S., Shin, Y.J., Ye, S.K., Kim, M.S., Park, J.W., 2008. Curcumin attenuates cytochrome P450 induction in response to 2,3,7,8-tetrachlorodibenzo-p-dioxin by ROS-dependently degrading AhR and ARNT. Cancer Science 99(12):2518—2524.

[36] Pollenz, R.S., 2007. Specific blockage of ligand-induced degradation of the Ah receptor by proteasome but not calpain inhibitors in cell culture lines from different species. Biochemical Pharmacology 74(1):131—143.

[37] Bock, K.W., 2017. Human and rodent aryl hydrocarbon receptor (AHR): from mediator of dioxin toxicity to physiologic AHR functions and therapeutic options. Biological Chemistry 398(4):455—464.

[38] McMillan, B.J., Bradfield, C.A., 2007. The aryl hydrocarbon receptor is activated by modified low-density lipoprotein. Proceedings of the National Academy of Sciences of the United States of America 104(4):1412—1417.

[39] Quintana, F.J., Sherr, D.H., 2013. Aryl hydrocarbon receptor control of adaptive immunity. Pharmacological Reviews 65(4):1148—1161.

[40] Oesch-Bartlomowicz, B., Huelster, A., Wiss, O., Antoniou-Lipfert, P., Dietrich, C., Arand, M., et al., 2005. Aryl hydrocarbon receptor activation by cAMP vs. dioxin: divergent signaling pathways. Proceedings of the National Academy of Sciences of the United States of America 102(26):9218—9223.

[41] Oury, F., Khrimian, L., Denny, C.A., Gardin, A., Chamouni, A., Goeden, N., et al., 2013. Maternal and offspring pools of osteocalcin influence brain development and functions. Cell 155(1):228—241.

[42] Zoch, M.L., Clemens, T.L., Riddle, R.C., 2016. New insights into the biology of osteocalcin. Bone 82:42—49.

[43] Boguslawski, G., Hale, L.V., Yu, X.P., Miles, R.R., Onyia, J.E., Santerre, R.F., et al., 2000. Activation of osteocalcin transcription involves interaction of protein kinase A- and protein kinase C-dependent pathways. Journal of Biological Chemistry 275(2):999—1006.

[44] Villafán-Bernal, J.R., Sánchez-Enríquez, S., Muñoz-Valle, J.F., 2011. Molecular modulation of osteocalcin and its relevance in diabetes (Review). International Journal of Molecular Medicine 28(3):283—293.

[45] Yu, X.P., Chandrasekhar, S., 1997. Parathyroid hormone (PTH 1-34) regulation of rat osteocalcin gene transcription. Endocrinology 138(8):3085—3092.

[46] Jang, W.G., Jeong, B.C., Kim, E.J., Choi, H., Oh, S.H., Kim, D.K., et al., 2015. Cyclic AMP response element-binding protein H (CREBH) mediates the inhibitory actions of tumor necrosis factor α in osteoblast differentiation by stimulating smad1 degradation. Journal of Biological Chemistry 290(21): 13556—13566.

[47] Sun, S., Hanzawa, F., Kim, D., Umeki, M., Nakajima, S., Sakai, K., et al., 2019. Circadian rhythm-dependent induction of hepatic lipogenic gene expression in rats fed a high-sucrose diet. Journal of Biological Chemistry 294(42):15206—15217.

[48] Izumida, Y., Yahagi, N., Takeuchi, Y., Nishi, M., Shikama, A., Takarada, A., et al., 2013. Glycogen shortage during fasting triggers liver-brain-adipose neurocircuitry to facilitate fat utilization. Nature Communications 4:2316.

[49] Cohen, J.C., Horton, J.D., Hobbs, H.H., 2011. Human fatty liver disease: old questions and new insights. Science 332(6037):1519—1523.

[50] Cheng, Y., Ma, Z., Kim, B.H., Wu, W., Cayting, P., Boyle, A.P., et al., 2014. Principles of regulatory information conservation between mouse and human. Nature 515(7527):371—375.

[51] Lo, R., Matthews, J., 2012. High-resolution genome-wide mapping of AHR and ARNT binding sites by ChIP-Seq. Toxicological Sciences 130(2):349—361.

[52] Nault, R., Fader, K.A., Ammendolia, D.A., Dornbos, P., Potter, D., Sharratt, B., et al., 2016. Dose-dependent metabolic reprogramming and differential gene expression in TCDD-elicited hepatic fibrosis. Toxicological Sciences 154(2):253—266.

[53] Rothhammer, V., Quintana, F.J., 2019. The aryl hydrocarbon receptor: an environmental sensor integrating immune responses in health and disease. Nature Reviews Immunology 19(3):184—197.

[54] Xiao, W., Son, J., Vorrink, S.U., Domann, F.E., Goswami, P.C., 2015. Ligand-independent activation of aryl hydrocarbon receptor signaling in PCB3-quinone treated HaCaT human keratinocytes. Toxicology Letters 233(3):258—266.

[55] Srivastava, A.K., Bhattacharyya, S., Li, X., Mohan, S., Baylink, D.J., 2001. Circadian and longitudinal variation of serum C-telopeptide, osteocalcin, and skeletal alkaline phosphatase in C3H/HeJ mice. Bone 29(4):361—367.

[56] Nakagawa, Y., Shimano, H., 2018. CREBH regulates systemic glucose and lipid metabolism. International Journal of Molecular Sciences 19(5):1396.

[57] Otani, T., Mizokami, A., Kawakubo-Yasukochi, T., Takeuchi, H., Inai, T., Hirata, M., 2020. The roles of osteocalcin in lipid metabolism in adipose tissue and liver. Advances in Biological Regulation 78:100752.

[58] Browner, M.F., Hwang, P.K., Fletterick, R.J., 1992. Cooperative binding is not required for activation of muscle phosphorylase. Biochemistry 31(46): 11291—11296.

[59] Pi, M., Xu, F., Ye, R., Nishimoto, S.K., Williams, R.W., Lu, L., et al., 2020. Role of GPRC6A in regulating hepatic energy metabolism in mice. Scientific Reports 10(1):7216.

[60] Zhang, M., Nie, X., Yuan, Y., Wang, Y., Ma, X., Yin, J., et al., 2021. Osteocalcin alleviates nonalcoholic fatty liver disease in mice through GPRC6A. The Internet Journal of Endocrinology 2021:9178616.

[61] Rutledge, A.C., Su, Q., Adeli, K., 2010. Apolipoprotein B100 biogenesis: a complex array of intracellular mechanisms regulating folding, stability, and lipoprotein assembly. Biochemistry and Cell Biology 88(2):251—267.

[62] Owen, J.B., 1999. Genetic aspects of body composition. Nutrition 15(7—8): 609—613.

[63] Silventoinen, K., Rokholm, B., Kaprio, J., Sørensen, T.I., 2010. The genetic and environmental influences on childhood obesity: a systematic review of twin and adoption studies. International Journal of Obesity 34(1):29—40.

